
U-DET: A MODIFIED U-NET ARCHITECTURE WITH BIDIRECTIONAL FEATURE NETWORK FOR LUNG NODULE SEGMENTATION

Nikhil Varma Keetha

Department of Physics
Indian Institute of Technology (Indian School of Mines) Dhanbad
Jharkand - 826004, India
keethanikhil@gmail.com

Samson Anosh Babu P

Department of CSE
Indian Institute of Technology (Indian School of Mines) Dhanbad
Jharkand - 826004, India
samson.enosh@gmail.com

Chandra Sekhara Rao Annavarapu

Department of CSE
Indian Institute of Technology (Indian School of Mines) Dhanbad
Jharkand - 826004, India
acsrao@iitism.ac.in

March 23, 2020

ABSTRACT

Early diagnosis and analysis of lung cancer involve a precise and efficient lung nodule segmentation in computed tomography (CT) images. However, the anonymous shapes, visual features, and surroundings of the nodule in the CT image pose a challenging problem to the robust segmentation of the lung nodules. This article proposes U-Det, a resource-efficient model architecture, which is an end to end deep learning approach to solve the task at hand. It incorporates a Bi-FPN (bidirectional feature network) between the encoder and decoder. Furthermore, it uses Mish activation function and class weights of masks to enhance segmentation efficiency. The proposed model is extensively trained and evaluated on the publicly available LUNA-16 dataset consisting of 1186 lung nodules. The U-Det architecture outperforms the existing U-Net model with the Dice similarity coefficient (DSC) of 82.82% and achieves results comparable to human experts.

Keywords Lung nodule segmentation · Convolutional neural network · Bidirectional feature network · Deep learning · Computer-aided diagnosis

1 Introduction

Most of the prominent cancer deaths are due to Lung Cancer, and it has a relatively low five-year survival rate of 18 % (Siegel et al., 2016). One of the primary causes of these pulmonary nodules formation is irregular and uncontrollable growth of cells in the lung parenchyma. Detection and analysis of these nodules in the lung tissue in an early phase drastically improve the chance of survival of the patient and facilitates efficient treatment (El-Baz and Suri, 2011).

Computed tomography (CT) scans are a widely used and highly accurate format for screening and analysis of lung nodules. These scans are obtained using multi-detector row CT scanners. Precise segmentation of the lung nodules is critical, as it has a significant effect on subsequent analysis results (MacMahon et al., 2005). However, for making an accurate diagnosis, a radiologist must check a CT scan containing about 150-500 slices, which is a very challenging and time-taking task (Way et al., 2010). Moreover, it is hard to differentiate between the internal lung structure and the nodules, especially when the nodule is on the lung wall or attached to the end of a vessel in the lung tissue. The robust segmentation of lung nodules using simple threshold and morphological-based methods is very difficult (Kubota et al., 2011) due to the large variation in size and types of lung nodules ranging from adhesion-type nodules (juxtaleural and juxta-vascular) to GGO (ground-glass opacity) nodules. Fig.1 illustrates various types of lung nodules.

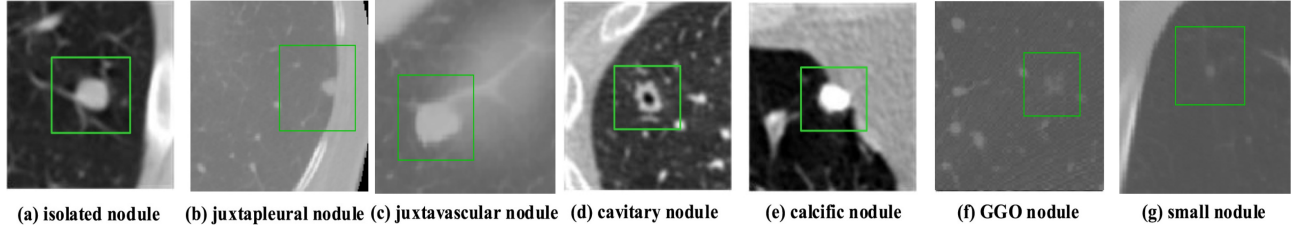


Figure 1: Illustrations of various types of lung nodules present in the CT scans. In (g), small nodule indicates a nodule of diameter ≤ 4 mm.

Another challenge in lung nodule segmentation is the segmentation of nodules with small diameter and intensity comparable to that of the surrounding noise. It is thereby hindering the downsampling potential of the segmentation network, where the network is unable to extract more in-depth network features that are semantic. This causes a significant impact on the accuracy of the extraction of feature maps of large nodules. For this reasons, a robust segmentation network is necessary to accommodate the large-scale nodule (various types) problem.

In the field of computer vision, convolutional neural networks (CNN) have recently become mainstream architecture. One such architecture, the U-Net, is an encoder-decoder like CNN architecture, which has shown exceptional results in the field of biomedical imaging on the task of segmentation (Ronneberger et al., 2015). Many modified U-Net architectures have achieved good results in different domains of biomedical imaging. However, CNN architectures implemented for the task of lung nodule segmentation are still immature. Therefore, the development of advanced architectures dealing with the shortcomings of previous architectures is essential.

To deal with the challenges of efficient feature extraction and adaption to heterogeneity of lung nodules, a modified U-Net architecture with a weighted bidirectional feature network (U-Det) is proposed, which is appropriate for the segmentation of many forms of lung nodules. The following elements are the list of technical contributions through this research.

1. The proposed U-Det model uses a bidirectional feature network, which functions as a feature enricher, integrating multi-scale feature fusion for efficient feature extraction.
2. The implementation of data augmentation to deal with the relatively small size of the dataset and thereby preventing the model from over-fitting and generalizing better on the task of segmentation and providing robust performance.
3. The implementation of Mish activation function and class weights of masks to enhance model training and segmentation efficiency.
4. The U-Det model can achieve high segmentation performance on small nodules and various other challenging cases of nodule segmentation.

2 Background and related work

This section describes several lung nodule segmentation strategies, like morphological methods, energy-based optimization techniques, region-growing processes, and machine learning methods that have been suggested in the past few years.

In morphological methods, morphological based-operations were applied for the task of removing the nodules attached to the vessels, and the isolation of lung nodules is done by selecting the connected region (Kostis et al., 2003). For improvement in separation of juxtaleural nodules from the lung wall, a morphological based-method combined with

the shape hypothesis has been proposed for the replacement of the morphological arrangement of fixed-size (Sargent and Park, 2017; Kuhnigk et al., 2006). However, lung nodule segmentation using morphological operations is very challenging (Diciotti et al., 2011).

In general, most region-growing methods are not capable of segmenting juxta-vascular and juxtapleural nodules and are just well suited to the isolation of calcified nodules (Kubota et al., 2011). To address this issue, Dehmeshki et al. offered a region-growing operation that operates on information on intensity, fuzzy connectivity, distance, and peripheral contrast (Dehmeshki et al., 2008). Here, a difficult task for these methods is the convergence condition. Also, irregular-shaped nodules are hard to process through region-growing methods due to the breach of the shape hypothesis.

The approach in energy based-optimization methods is to typically turn the task of segmentation into an energy minimization problem. For instance, in (Chan and Vese, 2001; Nithila and Kumar, 2016; Wang and Guo, 2016; Rebouças Filho et al., 2019; Farag et al., 2013), the authors have proposed a level set function for the characterization of the image, and the energy function reaches the minimum, once the segmented contour meets the boundary of the lung nodule. Also, the maximum flow problem was used in Ye et al. (2010); Boykov and Kolmogorov (2004); Mukherjee et al. (2017). Similar to the case of region-growing based operations, the presence of juxtapleural nodules and low contrast nodules such as GGO nodules drastically affects the output of these methods.

In the past decade, researchers in machine-learning field proposed hybrid models for classifying the lung nodules with high-level nodule segmentation feature maps (Lu et al., 2008, 2011). In one such case, for the classification task, Lu et al. established a collection of features maps with the invariance of translation and rotation (Lu et al., 2013). Another instance, Wu et al. proposed a culmination of texture and shape-dependent features for the classification of voxels, and a conditional random field (CRF) model was trained to classify voxels (Wu et al., 2010). Hu et al. performed the segmentation of the lungs and next carried out the Hessian matrix-based vascular feature extraction procedure to obtain the lung blood vessel mask. Then, the lung blood vessels were separated from the respective lung masks, and classification was achieved with the aid of a neural network (Hu and Menon, 2016). Jung et al.'s method performs GGO nodular segmentation centered on multi-phase models, which are asymmetric and deformable (Jung et al., 2018). Gonçalves et al. (2016) also developed a 3D large-scale nodule segmentation approach, based on the Hessian strategy.

Recently, to overcome the shortcomings of machine-learning based methods, Deep learning approaches have been proposed. In the deep learning approaches, CNN is a multi-layered neural network, which learns to map original image files and corresponding labels hierarchically, and the task of segmentation is modified into the classification of voxels similar to that used in the previous machine learning operations (Gao and Zhou, 2016; Shen et al., 2017). For instance, Wang et al. introduced the multi-view convolutional neural network (MVCNN) for nodule segmentation. The MVCNN is made up of three divisions of convolutional neural networks that are corresponding to three viewpoints of sagittal plane, axial plane, and coronal plane (Wang et al., 2017a). Zhao et al. have advocated an enhanced pyramid de-convolution network for enhanced performance on lung nodule segmentation. The architecture expertly blends low-level fine-grained characteristics with high-level functional characteristics (Zhao et al., 2019).

At the other end, Fully convolutional networks (Long et al., 2015) were a different method for the task of segmenting CT images. Few instances, Ronneberger et al. (2015) proposed 2D U-Net architecture and the 3D U-Net method advocated by Çiçek et al. (2016) are segmentation approaches which are better-adapted to biomedical imaging. Also, the central focused convolutional neural network(CF-CNN) proposed by Wang et al., which is a data-driven method without involving shape hypothesis, has shown strong performance for the segmentation of juxtapleural nodules (Wang et al., 2017b). Recently, Cao et al. (2020) proposed an approach of incorporating intensity features into the CNN architecture by implementing a Dual-branch residual network (DBResNet) to achieve attractive segmentation performance on lung nodules.

3 Methods

This section covers the methods that are applied in proposed model. It consists of the following three phases: (1) Model Architecture, (2) Data Augmentation, and (3) Training and post-processing. Fig.2 illustrates the pipeline of proposed model.

3.1 Model architecture

The model architecture is an End to End Deep learning approach for lung nodule segmentation. It takes inspiration from the encoder, decoder backbone of U-Net, and the feature enricher Bi-FPN, implemented in Efficient-Det. In this paper, the proposed model makes the use of U-Net based backbone network incorporated with a Bi-FPN for the task of lung nodule segmentation. Further, the fully convolutional network-based U-Net encoder takes the CT image, a slice of the CT scan, and outputs features at five corresponding depths, which are the respective inputs of the Bi-FPN. The

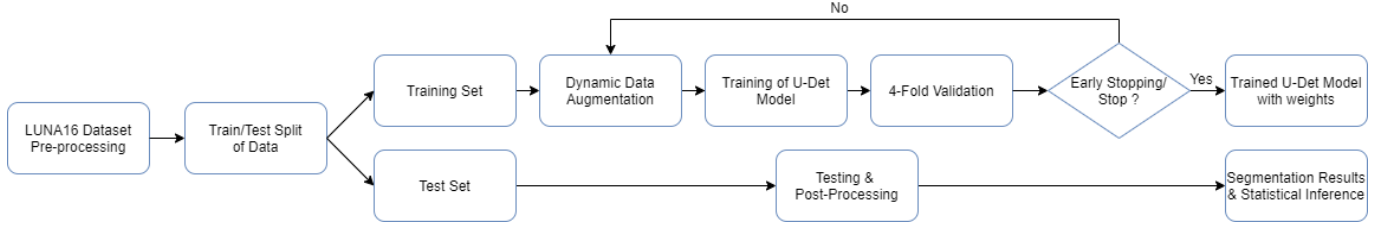


Figure 2: Flow chart representing the overview of proposed model pipeline.

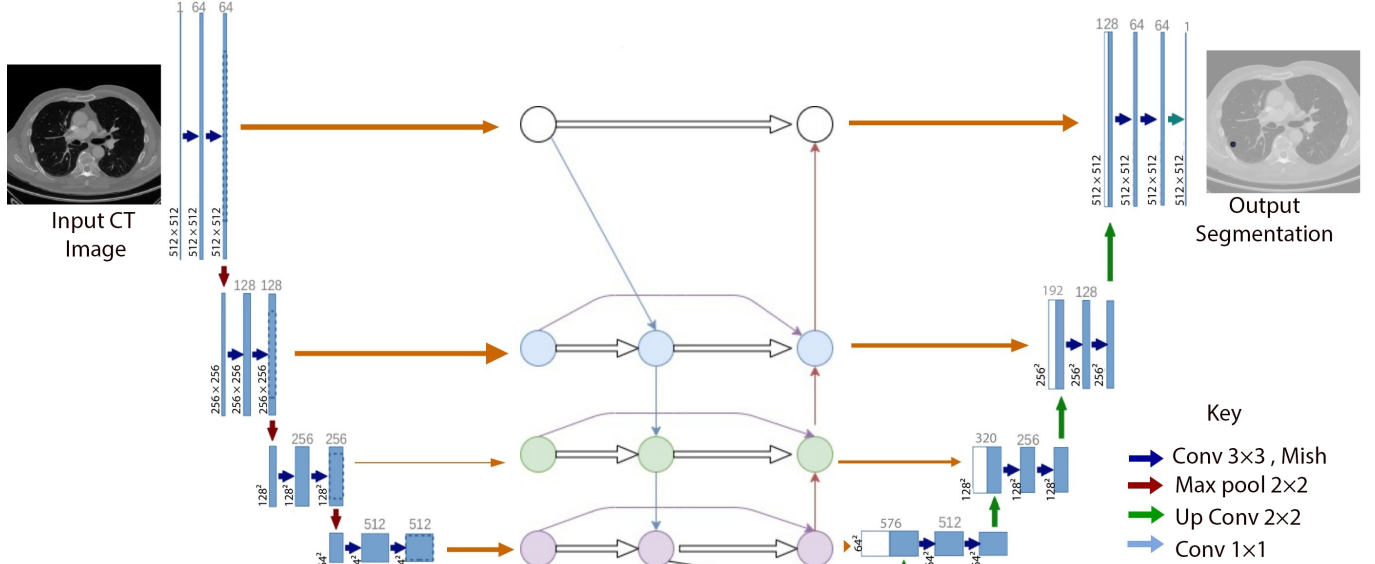


Figure 3: Illustration of the proposed U-Det model, where the convolutional neural network block between the downsampling and up-sampling sections represents the Bi-FPN. The numbers at each layer of the architecture indicate the shape of feature maps at each layer, respectively. The key indicates the representation of various operations that take place in the backbone architecture.

feature network’s outputs are combined respectively with a decoder architecture to obtain a combination of lower-level fine-grained features with high-level semantic features. The output mask represents lung nodules. Table.1 shows the corresponding layers of the model, along with their respective parameters. Fig.3 visualizes the proposed U-Det architecture.

3.1.1 Backbone U-Net architecture

The U-Net architecture is a convolutional network architecture for fast and precise segmentation of images. Recently, it has shown exceptional results in the field of biomedical image segmentation (Ronneberger et al., 2015). The proposed model uses a modified implementation of U-Net architecture to take a 512×512 image as an input and output a 512×512 mask. This architecture consists of two sections: the contraction and the expansion sections, which behave similarly to an encoder and decoder, respectively.

In the architecture, the contracting path has the typical architecture of a convolutional network, and consists of repeated application of two 3×3 convolutions (with ‘same’ padding), each followed by a non-linear Mish activation function and a 2×2 max-pooling operation of stride 2 for downsampling of the input image features. The number of feature channels is doubled at each downsampling step. The depth of the contraction path is five. Also, for the regularization of the model, a Dropout layer with a dropout factor of 0.5 has been used after the second 3×3 convolution block at depth

Table 1: The layers and respective network parameters of the U-Det model.

Layer name	Number of parameters
Contraction path :	
Conv2D×10, Mish	1.884×10^7
MaxPool2D×4	-
BiFPN :	
Conv2D×5	1.269×10^5
BatchNormalization×12	3072
ReLU×12, MaxPool2D×3	-
DepthwiseConv×7	4032
Expansion path :	
Conv2D×9, Mish	6.821×10^6
Conv2DTrans×4, Mish	2.786×10^6
Total parameters :	2.858×10^7

4. The corresponding sizes of features at the five depths of the contraction section are $512 \times 512 \times 64$, $256 \times 256 \times 128$, $128 \times 128 \times 256$, $64 \times 64 \times 512$, $32 \times 32 \times 1024$ where 64, 128, 256, 512, 1024 represents the number of channels.

The convolution process taking place at each layer of the model is denoted by the set of operations formulated below:

$$C[m, n] = (I \times k)[m, n] = \sum_i \sum_j k[i, j] \cdot I[m - i, n - j] \quad (1)$$

$$Z^{[l]} = W^{[l]} \cdot A^{[l-1]} + b^{[l]} \quad (2)$$

$$A^{[l]} = f^{[l]}(Z^{[l]}) \quad (3)$$

where, Eq.1 represents kernel convolution and Equations 2 and 3 denote the forward propagation process in CNN. Here in Eq.1, I and k denote the input image and kernel respectively. In Equations 2 and 3, $A^{[l]}$, $W^{[l]}$, $b^{[l]}$, $f^{[l]}$ indicate the activations, weights, bias, activation function of layer l respectively.

The features at the five depths are input into the feature network (Bi-FPN), and the output feature vectors are input into the expansion section. Each step in the expansion path consists of an upsampling of the feature map followed by a 2×2 convolution ("up-convolution"), which halves the number of feature channels at each depth. The feature vectors obtained after upsampling are concatenated with the corresponding feature vectors from the feature network. The concatenation operation is followed by two 3×3 convolutions ('same' padding) and each followed by the Mish activation function. In the final layer of the backbone network, the obtained $512 \times 512 \times 64$ feature map undergoes two 3×3 convolutions. It is followed by the Mish activation function and a final 1×1 convolution block, and finally, sigmoid activation function. Thereby obtaining logits corresponding to the mask of the input CT image of the shape 512×512 .

The network training aims to increase probability of right class of each voxel in the mask. To accomplish this, a weighted binary cross-entropy loss of each sample of training has been utilized. For the implementation of weighted binary cross-entropy, the positive pixels by the ratio of negative to positive voxels in the training set was weighted. Since the size of the positive class in a lung-nodule mask is relatively smaller than the size of the negative class, the class weight of the training set is positive thereby increasing the punishment for getting a positive value wrong. So the network will learn to be less biased towards outputting negative voxels due to the class imbalance in the masks. The weighted binary cross-entropy loss is formulated as follows:

$$Loss = \frac{-1}{N} \sum_{i=1}^N [\omega_p \times y_i \log \hat{y}_i + (1 - y_i) \log (1 - \hat{y}_i)] \quad (4)$$

where, N represents the number of samples, ω_p represents the positive prediction weights and \hat{y}_i indicates the prediction of the U-Det model.

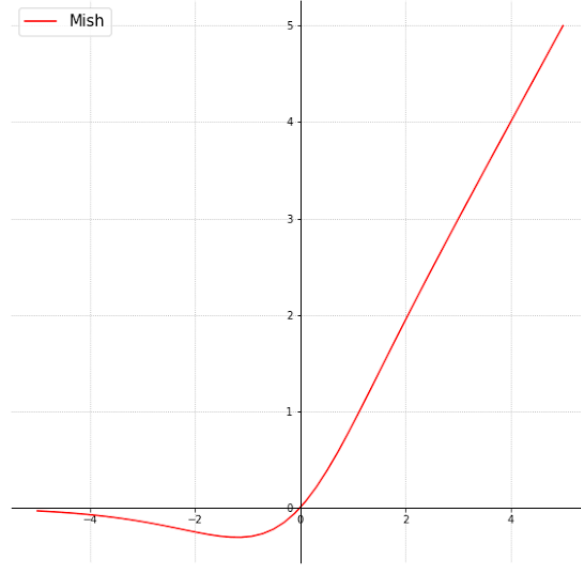


Figure 4: The graphical plot of Mish activation function.

3.1.2 Bi-FPN

The Bi-FPN is based on the conventional top-down FPN (Feature Pyramid Networks) approach (Lin et al., 2017). The Bi-FPN infuses efficient bidirectional cross-scale connections and weighted feature fusion into the model (Tan et al., 2019). Multi-scale feature fusion aims to fuse features at different resolutions to obtain efficient feature extractions. The one-way flow of information inherently limits conventional top-down FPN. A BiFPN does not consist of nodes that have only one input edge. If a node has only one input with no feature fusion, then it will contribute less to the feature network that aims to infuse different features. BiFPN also has one top-down and one bottom-up path, thereby allowing the bidirectional flow of features from one depth to the other in the feature network.

The incorporation of a bidirectional feature network aims to improve the feature extraction efficiency at each level of the backbone architecture and enrich the feature vectors, thereby allowing a fusion of lower-level fine-grained features and higher-level semantic features. As illustrated in Fig.3 the inputs of the Bi-FPN are the feature maps of the corresponding five depths of the contraction path of the backbone architecture. The outputs of Bi-FPN are fed into the expansion path of the backbone network.

The BiFPN also incorporates additional weight for each input during feature fusion, thereby allowing the network to learn the particular input feature importance. For dynamic learning behavior and accuracy fast normalized fusion (one of the methods of incorporating weights during feature fusion) is implemented (Tan et al., 2019). Also, for improvement of efficiency, depthwise separable convolution followed by batch normalization and non-linear activation function ReLU (Rectified Linear unit) are implemented. Through the bidirectional cross-scale connections, the Bi-FPN enriches the feature maps at each depth of the network and provides an efficient fusion of features across various depths of the encoder section of the U-Net backbone architecture.

3.1.3 Mish activation function

In the neural network, the activation function is the gateway to incorporating nonlinearity. It plays a pivotal part in the training and evaluation of deep neural networks. The widely used activation functions are ReLU, Sigmoid, Leaky ReLU, Tan hyperbolic, and recently introduced Swish. The approach implements a recent state of the art activation function Mish, which works better than ReLU and Swish across challenging datasets. Furthermore, the simplicity of Mish makes it a smooth implementation in neural networks (Misra, 2019).

Mish is a non-monotonic and smooth neural network activation function formulated as:

$$f(x) = x \cdot \tanh(\omega(x)) \quad (5)$$

where $\omega(x)$ is the softplus activation function given by $\ln(1 + e^x)$. Fig.4 illustrates the plot of the Mish activation function.

Mish implements a Self-Gating function, in which the input given to the gate is a scalar. The Self-Gating property helps replace activation functions such as ReLU (point-wise functions). Here, the input of the gating function is a scalar input with no requirement of modifying network parameters. In Tensorflow, the function definition of Mish is given by $x * tf.math.tanh(tf.softplus(x))$. Mish’s properties, like being above unbounded, below bounded, non-monotonic, and smooth, play a vital part in maximizing neural network outcomes. Hence, Mish enables considerable time improvements during the forward and backward pass on GPU (Graphics processing unit) inference, when CUDA (Compute Unified Device Architecture) is enabled, and improves the efficiency of the model.

3.2 Data augmentation

Medical image segmentation is constrained by the abundant availability of labeled training data. Data augmentation helps to prevent the model from over-fitting and helps in improving the generalization capability of the network on data outside the training set. It is vital in building robust deep learning pipelines (Mikołajczyk and Grochowski, 2018; Shorten and Khoshgoftaar, 2019). In medical imaging, the augmentations are provided to both the image and label equally, thereby creating warped versions of the training data.

The number of annotated CT scans (lung nodules) in datasets is relatively less compared to other domains of application of Deep Learning. Thus an efficient implementation of sampling strategies or data augmentation is crucial for the robust performance of neural networks. Recently, Wang et al. and Cao et al., implemented weighted sampling of training data to deal with the comparatively smaller size of the LIDC-IDRI dataset (Wang et al., 2017b; Cao et al., 2020). In the above method, the input slice of the CT scan is cropped to a smaller size with the help of a random weighted sampling strategy to increase the size of the training dataset.

The proposed model inputs CT images of size 512×512 , so a data augmentation strategy was followed instead of a sampling strategy to enhance the generalization potential and robustness of the proposed model. Data augmentation methods implemented in the proposed network are scale, flip, shift, rotate, and elastic deformations (LaLonde and Bagci, 2018). Further, salt and pepper noise (impulse noise) was added to the input slice of the CT image to improve the generalizability of the proposed neural network. Along with the noise, elastic transformation, random shear, zoom, and rotation, on the input image was implemented for maintaining the same input size. Thus by applying these small transformations to images during training, variety in the training dataset has been created and improved the robustness of the proposed U-Det model.

3.3 Training and post-processing

The training approach utilizes K-fold cross-validation (Bengio and Grandvalet, 2004) to obtain an accurate measure of the generalizing capability of the proposed model. To deal with the generation of augmented training CT images and corresponding ground truths, generators have been implemented for dynamic augmentation of input image and generation of corresponding ground truth labels. During model training, data augmentation and weighted binary cross-entropy deals with the data imbalance problem where the positive class was heavily over-weighted by the negative class in the masks.

In the training phase of proposed model, the ‘Adam’- model optimization algorithm (Kingma and Ba, 2014) was utilized with the following parameters : the initial learning rate is 0.0001, Beta_1 = 0.99, Beta_2 = 0.999, and decay rate is 1e-6. Also, a batch size of two samples was utilized to train the model. Further, the early stopping training strategy (Caruana et al., 2001) has been followed to prevent overfitting during the process of training the model.

In the post-processing phase, the proposed model has been designed to save the final obtained masks after the task of segmentation in a raw, metal (.mhd) format, which is one of the ways of storing volumetric data such as CT scans. Also, during testing, the proposed model has been designed to output qualitative figures, representing the final segmentation results and ground truth overlaid on the input CT image.

4 Data and experiments

This section deals with the data, implementation details, and assessment parameters (Evaluation metrics).

4.1 Data

For the experimentation and training of the proposed model, the approach utilizes the publicly available dataset of the Lung Nodule Analysis 2016 (LUNA16) grand challenge (Murphy et al., 2009; Jacobs et al., 2014; Setio et al., 2015; van Rikxoort et al., 2009). This dataset is derived from the public dataset Lung Image Database Consortium and Image

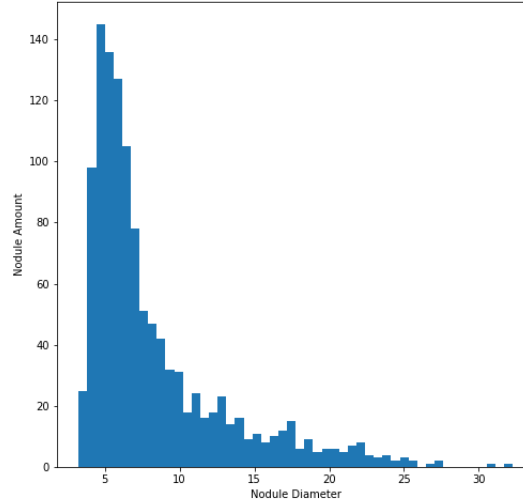


Figure 5: Histogram of lung nodules size across the LUNA16 dataset.

Table 2: Distribution of LUNA16 train and test sets. The values are indicated in the “mean \pm standard deviation” format.

Characteristics	Train Set (n=922)	Test Set (n=244)
Diameter(mm)	8.13 \pm 4.60	9.07 \pm 5.24
Margin	4.03 \pm 0.82	4.06 \pm 0.76
Spiculation	1.60 \pm 0.79	1.65 \pm 0.87
Lobulation	1.73 \pm 0.73	1.82 \pm 0.80
Subtlety	3.91 \pm 0.82	4.06 \pm 0.78
Malignancy	2.95 \pm 0.92	3.03 \pm 1.00

Note: The range for all distinctive feature values except diameter is between 1 to 5. Moreover, the ‘margin’ characteristic shows nodule edge clarity. ‘Spiculation’ and ‘lobulation’ indicate the shape characteristics of the nodule. ‘Subtlety’ explains the contrast between the nodule zone and its surrounding areas. ‘Malignancy’ reflects the possibility of this characteristic in a nodule.

Database Resource Initiative (LIDC-IDRI) (Armato III et al., 2011; Setio et al., 2017). It contains CT scans from the LIDC-IDRI database, where scans with a slice thickness 2.5 mm were excluded from the dataset. In total, 888 CT scans are included in the dataset. The LIDC-IDRI database contains annotations that were collected during a two-phase annotation process using four experienced radiologists. Here, the reference standard of the LUNA challenge consists of all nodules with a diameter greater than 3 mm accepted by at least three out of the four radiologists. The annotation file of the LUNA16 challenge contains annotations of 1186 nodules and also the enhanced annotations files indicating the various properties of the nodules. In Fig.5, the histogram of nodule amount and diameter of nodules is illustrated .

After pre-processing, a total of 1166 CT images with corresponding ground truth masks were created and partitioned into two training and test subsets as 922 and 244, respectively. We applied K-fold cross-validation of 4-folds during training process. As depicted in Table.2, the two subsets have identical statistical distribution in their clinical characteristics.

4.2 Evaluation metrics

The Dice similarity coefficient (DSC) is the key evaluation parameter for assessing the U-Det model’s segmentation performance. It is a commonly used metric to calculate the difference between the outcomes of two segmentations (Valverde et al., 2017; Havaei et al., 2017). In addition to the above metrics, the sensitivity (SEN) and positive predictive

value (PPV) have been used as auxiliary evaluation metrics. The evaluation metrics are formulated below:

$$DSC = \frac{2 \times V(Gt \cap Sv)}{V(Gt) + V(Sv)} \quad (6)$$

$$SEN = \frac{V(Gt \cap Sv)}{V(Gt)} \quad (7)$$

$$PPV = \frac{V(Gt \cap Sv)}{V(Sv)} \quad (8)$$

Where ‘‘Gt’’ represents the ground truth labels, ‘‘Sv’’ represents the segmentation results of the U-Det model. Here, volume size measured in voxel units is represented by ‘V.’

4.3 Implementation details

In this experiment, the Mish activation function (Section. 3.1.3) has been used for efficient training of the model, and also implementation of data augmentation was done on the LUNA16 training set to improve the robustness of the model (Section 3.2). Further, to prevent overfitting of the model, an early stopping training strategy was used; that is, if there is no more improvement in the performance of the model, then the model training will be stopped after an extra ten training epochs. Also, the strategy of reducing the learning rate of the optimizer on the model’s performance reaching a plateau was implemented. The experiment is based on the Tensorflow (Version 2.1) deep learning framework (GPU version), and Python 3.6 is the language used for coding and also used CUDA 10.2 (for GPU computing) for accelerated training. The experiment was carried out on the google cloud platform on a virtual instance equipped with 4 vCPUs, 15GB memory, and an SSD drive of 500 GB. During the training of the model, acceleration was done on the NVIDIA Tesla T4 GPU (14 GB video memory), and it takes about 8 hours of training to converge.

5 Results and discussion

This section covers the details of ablation study, overall performance of the proposed method, experimental comparison with other methods, and visualization of the results.

5.1 Ablation Study

An ablation experiment based on U-Net architecture has been designed. The ablation experiment verifies the effectiveness of each component in the proposed architecture. Table.3 shows the experimental results of the ablation study.

5.1.1 Effect of Mish Activation Function

In Table.3, U-Net + Mish indicates the incorporation of the Mish activation function instead of ReLU activation function of original U-Net architecture. The DSC score of the original U-Net is 77.84 %. After the implementation of the Mish function in U-Net, the DSC is observed to be 78.82 %. Further, an encoder consisting of the contraction path of the U-Net along with the Bi-FPN, was implemented. On adding the Mish activation function to the above architecture, the DSC was 80.22 %. Also, a version of the proposed U-Det model with ReLU is implemented, which performs marginally inferior to the mish version. It can be observed that the boost in performance due to Mish is nearly 1.3 %. Thus it is evident that the Mish activation function is useful in the U-Det model.

5.1.2 Effect of Bi-FPN

In Table.3, Encoder + Bi-FPN replaces the backbone U-Net architecture with only a contraction path and the Bi-FPN functioning as the feature enricher and decoder. It can be observed that this architecture shows improvement over the basic U-Net and achieves a DSC of 79.21 %. Also, the ReLU version of the U-Det model is an incorporation of the Bi-FPN in the U-Net architecture, and it is observed that the DSC score is 81.63 %, which is a significant improvement over the original U-Net.

In addition to the above, even though the Bi-FPN is less computationally expensive than the expansive path of the U-Net architecture in terms of parameters, the Encoder + Bi-FPN successfully incorporates multiple features fusion. The multi-feature fusion thereby allows simultaneous feature map enhancement, thereby showing improvement over the U-Net architecture. Also, the multiple implementations of Bi-FPN may serve as a decoder pathway, but it results in more complexity, computational expense, and does not result in significant improvement. Thus it can be inferred that the implementation of Bi-FPN between the expansive and contractive paths is very effectual in the proposed model.

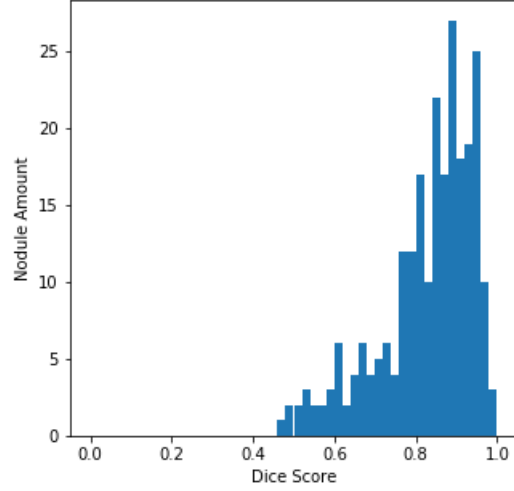


Figure 6: LUNA16 testset DSC distributions.

5.1.3 Effect of Bi-FPN + Expansion path

The combination of Bi-FPN and the expansion path (ReLU version of the U-Det model) has shown to be productive over the Encoder + Bi-FPN by exhibiting a DSC score of 81.63 %. The addition of the expansion path of U-Net to the Encoder + Bi-FPN model helps in proper upsampling of low-level features and a combination of feature maps from Bi-FPN. Thereby enabling the efficient fusion of high-level semantic features with low-level features.

5.1.4 Conclusion of the ablation study

In Table.3, on observation of the DSC score of the U-Det model (82.82 %), it is evident that the proposed U-Det shows significant improvement over U-Net. Effectiveness of all components and their culmination in the proposed model is verified through the ablation study.

Table 3: Ablation Study on LUNA16 testing dataset. The study is based upon the U-Net model.

Method	DSC(%)	SEN(%)	PPV(%)
U-Net	77.84 ± 21.74	77.98 ± 24.52	82.52 ± 21.53
U-Net + Mish	78.82 ± 22.01	78.97 ± 24.83	83.56 ± 21.80
Encoder + Bi-FPN	79.21 ± 12.49	84.40 ± 13.51	76.30 ± 14.42
Encoder + Bi-FPN + Mish	80.22 ± 12.33	85.47 ± 13.48	78.58 ± 14.34
U-Det + ReLU	81.63 ± 11.85	91.06 ± 13.96	77.94 ± 13.68
U-Det	82.82 ± 11.71	92.24 ± 14.14	78.92 ± 17.52

5.2 Overall performance

The histogram of the DSC values and the total amount of nodules, centered on every sample in the test set, is plotted, as illustrated in Fig.6, for better evaluation of the output of the U-Det model on test set. By observing Fig.6, it can be quickly concluded that most nodules have a DSC value greater than 0.8.

For verification of the effectiveness of the Bi-FPN, the DSC results were compared with the original U-Net architecture. The U-Net model had a DSC of 77.84%, whereas the proposed model has a DSC of 82.82%, shows robust performance in the task of segmentation. So having a lesser number of parameters than the original U-Net architecture, the proposed U-Det model has shown its potential for efficient feature extraction and segmentation.

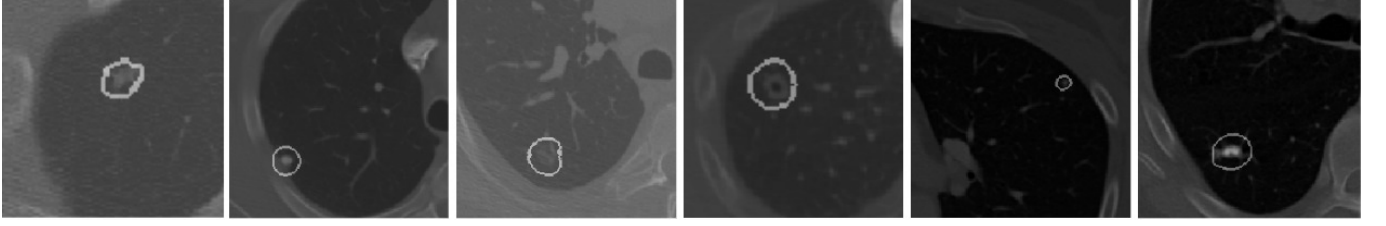


Figure 7: Visualization of segmentation results of the proposed U-Det model on heterogeneous types of lung nodules. The various types of lung nodules from left to right: isolated nodule, juxtapleural nodule, a nodule of GGO and juxta-vascular type, cavitory nodule, nodule of very small size, calcific nodule.

Table 4: The segmentation results of the proposed model on various cases such as attached and non-attached nodules, and nodules of large and small sizes.

	LUNA16 Test Set			
	Attached (n=56)	Non-Attached (n=188)	Diameter <6 mm (n=104)	Diameter >= 6 mm (n=140)
DSC (%)	81.82	83.11	83.40	82.40

Further, the segmentation results of difficult cases including attached nodules (juxtapleural and juxta-vascular) and nodules of small size were studied. The mean DSC outcomes can be seen in Table.4. By examining the experimental data shown in Table.4, it is evident that the U-Det model’s potential for robust segmentation is not dependent upon the type of nodule, and it performs exceptionally well on nodules of small size.

5.3 Experimental comparison

The results were compared with the results of other methods to depict the efficiency of the proposed method. The segmentation efficiency (DSC) of the four radiologists who worked on the LUNA16 (Derived from LIDC-IDRI) is known to be 82.25%, and it can be observed that U-Det model performs better than the human experts. Also, the proposed U-Det model was compared with models ranging from the original U-Net to various other recent convolution networks, including the recent DB-ResNet. (Cao et al., 2020).

In Table.5, the quantified results of the various methods are represented. The outputs are in “mean \pm standard deviation” format. As depicted in Table.5, the U-Det model has shown better performance over the existing segmentation methods. Therefore, the U-Det model performs segmentation efficiently, having fewer parameters than the given models.

Table 5: The quantitative segmentation results of proposed model compared to different types of model architectures.

Network Architecture	DSC (%)	SEN (%)	PPV (%)
FCN-UNET (Ronneberger et al., 2015)	77.84 \pm 21.74	77.98 \pm 24.52	82.52 \pm 21.53
CF-CNN (Wang et al., 2017b)	78.55 \pm 12.49	86.01 \pm 15.22	75.79 \pm 14.73
MC-CNN (Shen et al., 2017)	77.51 \pm 11.4	88.83 \pm 12.34	71.42 \pm 14.78
MV-CNN (Kang et al., 2017)	75.89 \pm 12.99	87.16 \pm 12.91	70.81 \pm 17.57
MV-DCNN (Wang et al., 2017a)	77.85 \pm 12.94	86.96 \pm 15.73	77.33 \pm 13.26
MCROI-CNN (Sun et al., 2017)	77.01 \pm 12.93	85.43 \pm 15.97	73.52 \pm 14.62
Cascaded-CNN (Havaei et al., 2017)	79.83 \pm 10.91	86.86 \pm 13.35	76.14 \pm 13.46
DB-ResNet (Cao et al., 2020)	82.74 \pm 10.19	89.35 \pm 11.79	79.64 \pm 13.54
U-Det	82.82 \pm 11.71	92.24 \pm 14.14	78.92 \pm 17.52

5.4 Visualization of results

Even though MV-CNN, FCN U-Net, MCROI-CNN, MC-CNN, Cascaded-CNN and CF-CNN achieved good results, DB-ResNet shows better performance over them. Although the DB-ResNet achieves good performance in various

cases, its performance is hindered in cases where the size of the nodule is less than 5mm (Cao et al., 2020) and in Fig.7, the performance of the U-Det model on challenging cases such as small nodules, cavitory nodules, juxta-vascular, and juxtapleural nodules from the LUNA16 dataset is illustrated. By this observation it is evident that the proposed model U-Det has shown efficient performance on various types of nodules, including nodules of size less than 5mm.

6 Conclusion

This paper proposes an efficient modified U-Net architecture using a weighted bidirectional feature network (U-Det) for the segmentation of lung nodules. The model extracts and decodes feature maps through the backbone U-Net architecture, and the Bi-FPN acts as a feature enricher by incorporating multi-scale feature fusion. Through evaluation and visualization of the results of the proposed method, the proposed method demonstrated encouraging precision in the segmentation of the lung nodules and obtained an 82.82% Dice similarity coefficient for the LUNA16 dataset. The U-Det model, in particular, successfully segments daunting cases such as cavitory nodules, GGO nodules, small nodules, and juxtapleural nodules. The future work focuses on developing a 3D Capsule Network based on the components of U-Det for fully automated malignancy classification of lung cancer.

Acknowledgments

The authors acknowledge the LUNA16 grand challenge organizers, the National Cancer Institute, and the Foundation for the National Institutes of Health and their critical role in the creation of the publicly available LUNA16 Database for this study. We also acknowledge the Kaggle Data Science Bowl 2017 for providing insightful information regarding pre-processing.

References

- Armato III, S.G., McLennan, G., Bidaut, L., McNitt-Gray, M.F., Meyer, C.R., Reeves, A.P., Zhao, B., Aberle, D.R., Henschke, C.I., Hoffman, E.A., et al., 2011. The lung image database consortium (lidc) and image database resource initiative (idri): a completed reference database of lung nodules on ct scans. *Medical physics* 38, 915–931.
- Bengio, Y., Grandvalet, Y., 2004. No unbiased estimator of the variance of k-fold cross-validation. *Journal of machine learning research* 5, 1089–1105.
- Boykov, Y., Kolmogorov, V., 2004. An experimental comparison of min-cut/max-flow algorithms for energy minimization in vision. *IEEE transactions on pattern analysis and machine intelligence* 26, 1124–1137.
- Cao, H., Liu, H., Song, E., Hung, C.C., Ma, G., Xu, X., Jin, R., Lu, J., 2020. Dual-branch residual network for lung nodule segmentation. *Applied Soft Computing* 86, 105934.
- Caruana, R., Lawrence, S., Giles, C.L., 2001. Overfitting in neural nets: Backpropagation, conjugate gradient, and early stopping, in: *Advances in neural information processing systems*, pp. 402–408.
- Chan, T.F., Vese, L.A., 2001. Active contours without edges. *IEEE Transactions on image processing* 10, 266–277.
- Çiçek, Ö., Abdulkadir, A., Lienkamp, S.S., Brox, T., Ronneberger, O., 2016. 3d u-net: learning dense volumetric segmentation from sparse annotation, in: *International conference on medical image computing and computer-assisted intervention*, Springer. pp. 424–432.
- Dehmeshki, J., Amin, H., Valdivieso, M., Ye, X., 2008. Segmentation of pulmonary nodules in thoracic ct scans: a region growing approach. *IEEE transactions on medical imaging* 27, 467–480.
- Diciotti, S., Lombardo, S., Falchini, M., Picozzi, G., Mascalchi, M., 2011. Automated segmentation refinement of small lung nodules in ct scans by local shape analysis. *IEEE Transactions on Biomedical Engineering* 58, 3418–3428.
- El-Baz, A., Suri, J.S., 2011. *Lung imaging and computer aided diagnosis*. CRC Press.
- Farag, A.A., El Munim, H.E.A., Graham, J.H., Farag, A.A., 2013. A novel approach for lung nodules segmentation in chest ct using level sets. *IEEE Transactions on Image Processing* 22, 5202–5213.
- Gao, W., Zhou, Z.H., 2016. Dropout rademacher complexity of deep neural networks. *Science China Information Sciences* 59, 072104.
- Gonçalves, L., Novo, J., Campilho, A., 2016. Hessian based approaches for 3d lung nodule segmentation. *Expert Systems with Applications* 61, 1–15.
- Havaei, M., Davy, A., Warde-Farley, D., Biard, A., Courville, A., Bengio, Y., Pal, C., Jodoin, P.M., Larochelle, H., 2017. Brain tumor segmentation with deep neural networks. *Medical image analysis* 35, 18–31.

- Hu, Y., Menon, P.G., 2016. A neural network approach to lung nodule segmentation, in: *Medical Imaging 2016: Image Processing*, International Society for Optics and Photonics. p. 97842O.
- Jacobs, C., van Rikxoort, E.M., Twellmann, T., Scholten, E.T., de Jong, P.A., Kuhnigk, J.M., Oudkerk, M., de Koning, H.J., Prokop, M., Schaefer-Prokop, C., et al., 2014. Automatic detection of subsolid pulmonary nodules in thoracic computed tomography images. *Medical image analysis* 18, 374–384.
- Jung, J., Hong, H., Goo, J.M., 2018. Ground-glass nodule segmentation in chest ct images using asymmetric multi-phase deformable model and pulmonary vessel removal. *Computers in biology and medicine* 92, 128–138.
- Kang, G., Liu, K., Hou, B., Zhang, N., 2017. 3d multi-view convolutional neural networks for lung nodule classification. *PLoS one* 12.
- Kingma, D.P., Ba, J., 2014. Adam: A method for stochastic optimization. *arXiv preprint arXiv:1412.6980*.
- Kostis, W.J., Reeves, A.P., Yankelevitz, D.F., Henschke, C.I., 2003. Three-dimensional segmentation and growth-rate estimation of small pulmonary nodules in helical ct images. *IEEE transactions on medical imaging* 22, 1259–1274.
- Kubota, T., Jerebko, A.K., Dewan, M., Salganicoff, M., Krishnan, A., 2011. Segmentation of pulmonary nodules of various densities with morphological approaches and convexity models. *Medical Image Analysis* 15, 133–154.
- Kuhnigk, J.M., Dicken, V., Bornemann, L., Bakai, A., Wormanns, D., Krass, S., Peitgen, H.O., 2006. Morphological segmentation and partial volume analysis for volumetry of solid pulmonary lesions in thoracic ct scans. *IEEE Transactions on Medical Imaging* 25, 417–434.
- LaLonde, R., Bagci, U., 2018. Capsules for object segmentation. *arXiv preprint arXiv:1804.04241*.
- Lin, T.Y., Dollár, P., Girshick, R., He, K., Hariharan, B., Belongie, S., 2017. Feature pyramid networks for object detection, in: *Proceedings of the IEEE conference on computer vision and pattern recognition*, pp. 2117–2125.
- Long, J., Shelhamer, E., Darrell, T., 2015. Fully convolutional networks for semantic segmentation, in: *Proceedings of the IEEE conference on computer vision and pattern recognition*, pp. 3431–3440.
- Lu, L., Barbu, A., Wolf, M., Liang, J., Salganicoff, M., Comaniciu, D., 2008. Accurate polyp segmentation for 3d ct colonography using multi-staged probabilistic binary learning and compositional model, in: *2008 IEEE Conference on Computer Vision and Pattern Recognition*, IEEE. pp. 1–8.
- Lu, L., Bi, J., Wolf, M., Salganicoff, M., 2011. Effective 3d object detection and regression using probabilistic segmentation features in ct images, in: *CVPR 2011*, IEEE. pp. 1049–1056.
- Lu, L., Devarakota, P., Vikal, S., Wu, D., Zheng, Y., Wolf, M., 2013. Computer aided diagnosis using multilevel image features on large-scale evaluation, in: *International MICCAI Workshop on Medical Computer Vision*, Springer. pp. 161–174.
- MacMahon, H., Austin, J.H., Gamsu, G., Herold, C.J., Jett, J.R., Naidich, D.P., Patz Jr, E.F., Swensen, S.J., 2005. Guidelines for management of small pulmonary nodules detected on ct scans: a statement from the fleischner society. *Radiology* 237, 395–400.
- Mikołajczyk, A., Grochowski, M., 2018. Data augmentation for improving deep learning in image classification problem, in: *2018 international interdisciplinary PhD workshop (IIPhDW)*, IEEE. pp. 117–122.
- Misra, D., 2019. Mish: A self regularized non-monotonic neural activation function. *arXiv preprint arXiv:1908.08681*.
- Mukherjee, S., Huang, X., Bhagalia, R.R., 2017. Lung nodule segmentation using deep learned prior based graph cut, in: *2017 IEEE 14th International Symposium on Biomedical Imaging (ISBI 2017)*, IEEE. pp. 1205–1208.
- Murphy, K., van Ginneken, B., Schilham, A.M., De Hoop, B., Gietema, H., Prokop, M., 2009. A large-scale evaluation of automatic pulmonary nodule detection in chest ct using local image features and k-nearest-neighbour classification. *Medical image analysis* 13, 757–770.
- Nithila, E.E., Kumar, S., 2016. Segmentation of lung nodule in ct data using active contour model and fuzzy c-mean clustering. *Alexandria Engineering Journal* 55, 2583–2588.
- Rebouças Filho, P.P., da Silva Barros, A.C., Almeida, J.S., Rodrigues, J., de Albuquerque, V.H.C., 2019. A new effective and powerful medical image segmentation algorithm based on optimum path snakes. *Applied Soft Computing* 76, 649–670.
- van Rikxoort, E.M., de Hoop, B., Viergever, M.A., Prokop, M., van Ginneken, B., 2009. Automatic lung segmentation from thoracic computed tomography scans using a hybrid approach with error detection. *Medical physics* 36, 2934–2947.
- Ronneberger, O., Fischer, P., Brox, T., 2015. U-net: Convolutional networks for biomedical image segmentation, in: *International Conference on Medical image computing and computer-assisted intervention*, Springer. pp. 234–241.

- Sargent, D., Park, S.Y., 2017. Semi-automatic 3d lung nodule segmentation in ct using dynamic programming, in: *Medical Imaging 2017: Image Processing*, International Society for Optics and Photonics. p. 101332R.
- Setio, A.A., Jacobs, C., Gelderblom, J., van Ginneken, B., 2015. Automatic detection of large pulmonary solid nodules in thoracic ct images. *Medical physics* 42, 5642–5653.
- Setio, A.A.A., Traverso, A., De Bel, T., Berens, M.S., van den Bogaard, C., Cerello, P., Chen, H., Dou, Q., Fantacci, M.E., Geurts, B., et al., 2017. Validation, comparison, and combination of algorithms for automatic detection of pulmonary nodules in computed tomography images: the luna16 challenge. *Medical image analysis* 42, 1–13.
- Shen, W., Zhou, M., Yang, F., Yu, D., Dong, D., Yang, C., Zang, Y., Tian, J., 2017. Multi-crop convolutional neural networks for lung nodule malignancy suspiciousness classification. *Pattern Recognition* 61, 663–673.
- Shorten, C., Khoshgoftaar, T.M., 2019. A survey on image data augmentation for deep learning. *Journal of Big Data* 6, 60.
- Siegel, R.L., Miller, K.D., Jemal, A., 2016. *Cancer statistics, 2016*. CA: a cancer journal for clinicians 66, 7–30.
- Sun, W., Zheng, B., Qian, W., 2017. Automatic feature learning using multichannel roi based on deep structured algorithms for computerized lung cancer diagnosis. *Computers in biology and medicine* 89, 530–539.
- Tan, M., Pang, R., Le, Q.V., 2019. Efficientdet: Scalable and efficient object detection. *arXiv preprint arXiv:1911.09070*.
- Valverde, S., Oliver, A., Roura, E., González-Villà, S., Pareto, D., Vilanova, J.C., Ramió-Torrentà, L., Rovira, À., Lladó, X., 2017. Automated tissue segmentation of mr brain images in the presence of white matter lesions. *Medical image analysis* 35, 446–457.
- Wang, J., Guo, H., 2016. Automatic approach for lung segmentation with juxta-pleural nodules from thoracic ct based on contour tracing and correction. *Computational and mathematical methods in medicine* 2016.
- Wang, S., Zhou, M., Gevaert, O., Tang, Z., Dong, D., Liu, Z., Tian, J., 2017a. A multi-view deep convolutional neural networks for lung nodule segmentation, in: *2017 39th Annual International Conference of the IEEE Engineering in Medicine and Biology Society (EMBC)*, IEEE. pp. 1752–1755.
- Wang, S., Zhou, M., Liu, Z., Liu, Z., Gu, D., Zang, Y., Dong, D., Gevaert, O., Tian, J., 2017b. Central focused convolutional neural networks: Developing a data-driven model for lung nodule segmentation. *Medical image analysis* 40, 172–183.
- Way, T., Chan, H.P., Hadjiiski, L., Sahiner, B., Chughtai, A., Song, T.K., Poopat, C., Stojanovska, J., Frank, L., Attili, A., et al., 2010. Computer-aided diagnosis of lung nodules on ct scans: Roc study of its effect on radiologists' performance. *Academic radiology* 17, 323–332.
- Wu, D., Lu, L., Bi, J., Shinagawa, Y., Boyer, K., Krishnan, A., Salganicoff, M., 2010. Stratified learning of local anatomical context for lung nodules in ct images, in: *2010 IEEE Computer Society Conference on Computer Vision and Pattern Recognition*, IEEE. pp. 2791–2798.
- Ye, X., Beddoe, G., Slabaugh, G., 2010. Automatic graph cut segmentation of lesions in ct using mean shift superpixels. *International journal of biomedical imaging* 2010.
- Zhao, X., Sun, W., Qian, W., Qi, S., Sun, J., Zhang, B., Yang, Z., 2019. Fine-grained lung nodule segmentation with pyramid deconvolutional neural network, in: *Medical Imaging 2019: Computer-Aided Diagnosis*, International Society for Optics and Photonics. p. 109503S.